Asari, S., Wardinski, I. (2015): On magnetic estimation of Earth's core angular momentum variation. - *Journal of Geophysical Research*, *120*, 10, pp. 6740—6757.

DOI: http://doi.org/10.1002/2014JB011458

AGU PUBLICATIONS

JGR

Journal of Geophysical Research: Solid Earth

RESEARCH ARTICLE
10.1002/2014JB011458

On magnetic estimation of Earth's core angular momentum variation

S. Asari[1,2] and I. Wardinski[2]

[1]Institute for Mathematics, University of Potsdam, Potsdam, Germany, [2]Helmholtz Centre Potsdam, GFZ German Research Centre for Geosciences, Potsdam, Germany

Key Points:
- Estimation of core angular momentum (CAM) variation is systematically studied
- Stronger core flow constraints steepen estimates of the CAM secular trend
- Estimation of the 6 year CAM variation is subject to multiple sources of uncertainty

Correspondence to:
S. Asari,
asari@gfz-potsdam.de

Citation:
Asari, S., and I. Wardinski (2012), On magnetic estimation of Earth's core angular momentum variation, *J. Geophys. Res. Solid Earth*, *120*, 6740–6757, doi:10.1002/2014JB011458.

Received 14 JUL 2014
Accepted 20 SEP 2015
Accepted article online 28 SEP 2015
Published online 21 OCT 2015

Abstract We study systematically the estimation of Earth's core angular momentum (CAM) variation between 1962.0 and 2008.0 by using core surface flow models derived from the recent geomagnetic field model C^{3}FM2. Various flow models are derived by changing four parameters that control the least squares flow inversion. The parameters include the spherical harmonic (SH) truncation degree of the flow models and two Lagrange multipliers that control the weights of two additional constraints. The first constraint forces the energy spectrum of the flow solution to follow a power law $\propto l^{-p}$, where l is the SH degree and p is the fourth parameter. The second allows to modulate the solution continuously between the dynamical states of tangential geostrophy (TG) and tangential magnetostrophy (TM). The calculated CAM variations are examined in reference to two features of the observed length-of-day (LOD) variation, namely, its secular trend and 6 year oscillation. We find flow models in either TG or TM state for which the estimated CAM trends agree with the LOD trend. It is necessary for TM models to have their flows dominate at planetary scales, whereas TG models should not be of this scale; otherwise, their CAM trends are too steep. These two distinct types of flow model appear to correspond to the separate regimes of previous numerical dynamos that are thought to be applicable to the Earth's core. The phase of the subdecadal CAM variation is coherently determined from flow models obtained with extensively varying inversion settings. Multiple sources of model ambiguity need to be allowed for in discussing whether these phase estimates properly represent that of Earth's CAM as an origin of the observed 6 year LOD oscillation.

1. Introduction

The observed variations of Earth rotation originate from angular momentum exchanges between the solid and fluid parts of the Earth, aside from secular changes due to tidal forces. The variations shorter than a couple of years are attributed quite certainly to the atmosphere and ocean angular momentum changes that are modeled from direct observations [*Holme and de Viron*, 2013]. On longer timescales, the dominating cause of Earth rotation variations is likely to be dynamical interactions across the core-mantle boundary. From 1962 on, records of the excess length of day (LOD) are provided online by the International Earth Rotation and Reference Systems Service (http://www.iers.org), with an accuracy on the order of ~0.1 to 1 ms up until 1983 and ~0.01 ms thereafter. Furthermore, the tidal, atmospheric, and oceanic effects have been subtracted to have the residual Λ_o that is likely due to variations of the core angular momentum (CAM) [*Holme and de Viron*, 2005, 2013]. In this paper, we refer to Λ_o simply as observed LOD variation.

The past 50 years may be suitable for studying the CAM variation more in detail, as it is supported by the reliable Λ_o. Magnetic data are also supplied by a network of ground-based observatories substantially improved in 1957. One of the geomagnetic field models recently built for this period is C^{3}FM2 [*Wardinski and Lesur*, 2012]. This is a model of the time-dependent main field, which we believe is suitable for studying the core flow from 1957 to 2008. It is constructed from ground-based secular variation (SV) data, supplemented by CHAMP main field data for 2004.0.

In this work, the CAM variation is investigated using core flow models estimated from the variant of C^{3}FM2 derived without imposing the frozen-flux constraint (we refer to it simply as C^{3}FM2 and to the other variant under the frozen-flux constraint as FF-C^{3}FM2). The CAM variation estimation is subject to ambiguity due to that of core flow modeling from a magnetic field model [*Holme*, 2007]. The estimates vary substantially with flow models [*Holme and Olsen*, 2006; *Olsen and Mandea*, 2008]. The ambiguity is such that the flow models can even be constrained so that their accompanying CAM variation accounts almost perfectly for the decadal LOD

observation [*Holme*, 1998]. The existence of such a flow model may not prove straightforwardly the hypothesis of core-mantle angular momentum exchange, but at least the hypothesis is thereby ensured not to be ruled out. It is still worth comparing "purely magnetic" LOD predictions and the "purely geodetic" LOD observation, as they are independent geophysical data sets. The comparison has actually been made for varying purposes: verifying the core-mantle angular momentum exchange [*Jackson et al.*, 1993; *Wardinski et al.*, 2008], discussing the core dynamics [*Gillet et al.*, 2010], and evaluating magnetically estimated flow models [*Holme and Olsen*, 2006].

The purpose of this work does not belong to any of the above. We do not seek for any specific flow model that is "qualified"—statistically consistent with magnetic observations, theoretically likely for the deep Earth, and hence suitable for interpreting observations or discussing underlying physics. We rather focus on investigating the variability of magnetically estimated CAM variation. To reveal how flow inversion setting influences subsequent estimates, a systematic analysis is performed by deriving a diverse set of flow models from a single magnetic field model C^3FM2. In particular, we study changes of CAM estimates with respect to individual tuning parameters of the flow inversion by varying them within a broad range. The explored range is such that some of the inversions, especially those neighboring end-members, produce models which may be considered no longer qualified for one or more reasons (depending on requirements a priori assumed). Hence, we restrict this study only to inducing the general tendency for the estimation method from the whole range of systematic inversions. Our findings could nevertheless be useful, when studying the Earth rotation variation or core dynamics by applying only one or a few selections of qualified models, such as in our separate paper (I. Wardinski and S. Asari, Sub-decadal and decadal variations of Earth's rotation and outer core flow, submitted to *Geophysical Journal International*, 2015).

We particularly address the following two issues, each regarding separate features of the observed LOD variation. First, we examine the secular trend of estimated CAM over the investigated period. It has been pointed out that estimates of CAM trend are significantly inconsistent with the LOD observation, when flow models are used that are built by imposing a strong constraint, such as tangential geostrophy (TG) or quasi-geostrophy [*Wardinski*, 2005; *Gillet et al.*, 2009]. These trend estimates are made to discuss Earth phenomena with flow models only in specific prior beliefs. We systematically seek different inversion settings for those tending to yield CAM estimates preferable for the observed LOD trend. Second, we evaluate magnetic detectability of the subdecadal CAM variations. Besides the 6 year periodicity in the observed LOD, there have also been implications for the presence of rapid CAM oscillations from magnetic field observations [*Silva et al.*, 2012; *Brown et al.*, 2013] or a numerical experiment [*Mound and Buffett*, 2006]. However, the expected amplitude of corresponding CAM oscillations is so small that a concern remains—historical observations of noisy magnetic field may fail to give a sufficient sensitivity for the rapid CAM oscillations. Analyzing a wide variety of CAM estimates in our systematic inversions, we discuss whether the 6 year CAM variation can be robustly resolved from C^3FM2.

2. Core Angular Momentum Variation and Length-of-Day Prediction

We examine *Jault et al.* [1988] method for computing CAM variation from a temporally continuous core surface flow model. The observed decadal and subdecadal CAM variations may result principally from rotation variations of Taylor cylinders, which may be derived from equatorially symmetric zonal toroidal part of the core surface flow. By approximating such cylinders to exist even within the inner core tangent cylinder, it is possible to analytically integrate the angular momentum variations over the whole core. This leads to a simple expression given in terms only of two zonal toroidal coefficients, t_1^0 and t_3^0, at spherical harmonic (SH) degrees 1 and 3, respectively.

For discussing the calculated CAM variation, it is useful to translate it into the LOD variation Λ_J in millisecond, assuming an angular momentum conservation between the core and mantle. The fundamental formula is given by *Jackson et al.* [1993] and computed practically by

$$\Lambda_J = 1.138 \left(t_1^0 + \frac{12}{7} t_3^0 \right), \tag{1}$$

where the unit of the flow coefficients is km/yr [*Jackson*, 1997]. Only the time variation of the formula (1) is to be discussed. The offset has no physical significance, not only because the steady part of CAM is irrelevant to the observed LOD variation but also because the offset may fail to describe the steady part of CAM. Unless the core is in a quasi-geostrophic state [*Pais and Jault*, 2008; *Gillet et al.*, 2009], the CAM can be carried by

the quasi-static convection, consisting of flows varying along the direction parallel to Earth rotation axis and hence unknown from the core surface flow.

3. Magnetic Estimation of the Core Surface Flow

We outline the setting of our least squares inversion for temporally continuous core surface flow, which is subsequently used to calculate the CAM variation in the form of LOD prediction (1). For this linear inversion we adopt the method and assumptions that have been used in previous studies. In this paper, we just reference past studies in which the details are sufficiently given along with mathematical formulations, instead of describing them at length.

3.1. Core Surface Flow Inversion

Our flow inversion is carried out with the spectral method in space, where all involved quantities are expanded in Schmidt's quasi-normalized spherical harmonics. The spherical harmonic (SH) degree l defines the spatial scale over the spherical surface with the core radius 3485 km. In this paper, following *Pais and Jault* [2008], we use the terms "large scale," "intermediate scale," and "small scale" to refer to the scales corresponding to $1 \le l \le 5$, $6 \le l \le 14$, and $l \ge 15$, respectively. The horizontal core surface flow $\vec{u}_H$ is parametrized with SH coefficients of its toroidal and poloidal scalar functions. The truncation degree L of the expanded series is varied in this study within the range between 14 and 37. To build a time-dependent flow model, each SH flow coefficient is expanded in time on the basis of the B-spline function of order 6, the knot locations being the same as those of C^{3}FM2 (evenly distributed with the intervals of ~1.4 years). The temporal evolution of each SH coefficient is expressed by $N_t = 42$ parameters.

Our inversion solution for those flow coefficients is obtained by minimizing the functional

$$\mathcal{N}_{\mathrm{FF}} + \lambda_{\mathrm{TM}}\mathcal{N}_{\mathrm{TM}} + \lambda_{\mathrm{TG}}\mathcal{N}_{\mathrm{TG}} + \lambda_p\mathcal{N}_p + \lambda_{\mathrm{dt}}\mathcal{N}_{\mathrm{dt}}\,. \tag{2}$$

Each semipositive definite L2 norm $\mathcal{N}_{(\cdot)}$ and its corresponding Lagrange multiplier $\lambda_{(\cdot)}$ (in yr^2/km^2) are detailed below in this subsection. The maximum number of the model parameters to be simultaneously determined sums up to $2N_tL(L+2) = 121,212$ when $L = 37$. Despite its large dimension, solutions can still be derived by numerically solving the normal equation using Cholesky decomposition of the involved matrix.

The principal constraint on the flow $\vec{u}_H$ is based on the radial component of the diffusionless induction equation at the core surface [*Holme*, 2007]

$$\dot{B}_r = -\nabla_H \cdot (B_r\vec{u}_H)\,, \tag{3}$$

in which the radial component B_r of the geomagnetic main field (MF) and its first time derivative $\dot{B}_r$ are involved. The first norm $\mathcal{N}_{\mathrm{FF}}$ in (2) stands for a weighted squared difference between C^{3}FM2 SV and the model prediction averaged over the model period. The prediction is given at the Earth's surface level (the spherical surface with the radius of 6371.2 km) by upward continuing the radial field variation $\dot{B}_r$ generated by the interaction of B_r and $\vec{u}_H$ as in (3). The norm is nondimensionalized by introducing weights W_l in yr^2/nT^2, which are dependent on SH degree l alone (see section 2.2 for W_l). As in most previous flow inversions, B_r is mapped at the core surface after the downward continuation of C^{3}FM2 MF, which is assumed to be free from variance.

We additionally impose physical constraints in our inversion. They are tangential magnetostrophy (TM) constraint and tangential geostrophy (TG) constraint, implemented respectively through the seminorms $\mathcal{N}_{\mathrm{TM}}$ and $\mathcal{N}_{\mathrm{TG}}$ in (2). $\mathcal{N}_{\mathrm{TM}}$ represents the temporally averaged kinetic energy of the non-TM flow, a subset of general flow $\vec{u}_H$ that does not satisfy the TM constraint at the core surface [*Jackson*, 1996]

$$2\rho\Omega\nabla_H \cdot (\cos\theta\vec{u}_H) = -\nabla_H \cdot (B_r\vec{j}_H)\,, \tag{4}$$

where known quantities are the mean core fluid density ρ ($= 1.2 \times 10^4$kg/m^3), the mantle's angular velocity Ω ($= 7.3 \times 1.0^{-5}$s^{-1}), and B_r mapped from C^{3}FM2 MF the same way as done in the induction equation (3). $\vec{j}_H$ is the unknown horizontal electrical current. $\mathcal{N}_{\mathrm{TM}}$ is actually derived from a "non-TM flow basis" set, obtained by eigenvalue decomposing the matrix connecting $\vec{u}_H$ and $\vec{j}_H$ in (4) [*Asari and Lesur*, 2011]. To ensure physical plausibility of resulting models, we fix λ_{TM} at such a large value that the non-TM flow is entirely eliminated from our models. $\mathcal{N}_{\mathrm{TG}}$ represents the temporally averaged kinetic energy of the non-TG flow, a set of TM flow

satisfying (4) but not satisfying the TG constraint $2\rho\Omega\nabla_H \cdot (\cos\theta \vec{u}_H) = 0$ [*Le Mouël*, 1984]. Note that the TG constraint is a special case of (4) where the Lorentz term does not play a role, as is the case with $\vec{j}_H = 0$, for instance. For our systematic inversions, we leave λ_{TG} variable. Thus, our flow models always belong to the class of TM flow, whether it is strictly TG flow or far from it.

We regularize the inversion by adding a constraint on the kinetic spectrum of the flow. Here we adopt a power law constraint introduced by *Pais and Hulot* [2000] for the sake of our systematic analysis; the flow solution is constrained to have an energy spectrum that obeys a power law $\propto l^{-p}$. This is actually done by including the norm $\mathcal{N}_p$ in (2), assuming that the flow coefficients are uncorrelated with one another and that their variances about zero means are proportional to $l^{p+1}(l+1)$, as a function of the SH degree l alone. We vary the value of p in the range between −1 and 1. Note that $p = -1$ corresponds to the inversion minimizing the flow kinetic energy integrated over the core surface and $p = 1$ to the regularization introduced and implemented by *Gillet et al.* [2009] ($p = 3$ would correspond to the so-called Bloxham strong norm [*Bloxham*, 1988]).

Finally, we weakly damp the time derivative of our flow solutions. $\mathcal{N}_{\mathrm{dt}}$ in (2) is the energy of flow acceleration averaged over the space and time, and λ_{dt} is fixed at a minimum value yet enough to stabilize the temporal behaviors near the ends of the model period.

After all, we are left with four controlling parameters L, p, λ_{TG}, and λ_p.

3.2. Magnetic Field

The radial magnetic field B_r at the core surface in (3) and (4) may be written as $B_r = \overline{B_r} + B_r^{(k)}$, divided into large- and intermediate-scale components $\overline{B_r}$ and small-scale components $B_r^{(k)}$ [*Gillet et al.*, 2009]. We map $\overline{B_r}$ by using C^{3}FM2 Gauss coefficients up to SH degree 14. For some inversions, the field is supplemented by $B_r^{(k)}$, which we generate by synthesizing all Gauss coefficients at degrees $15 \le l \le L$, postulating a stochastic process for their temporal evolutions [*Gillet et al.*, 2009]. Instead of the Gaussian process assumed by *Gillet et al.* [2009], we randomly generate time series of the small-scale Gauss coefficients such that (1) the temporal average is zero and (2) the autocorrelation has an exponential form $\sigma^2 \exp(-|\Delta t|/\tau)$, where σ^2 is the variance and Δt is the time shift, which is known to be compatible with the large-scale field [see, e.g., *Hongre et al.*, 1998]. The relaxation time τ is set at 20 years for all coefficients, roughly according to the autocorrelations of C^{3}FM2 Gauss coefficients at degrees 10 to 14. Following *Gillet et al.* [2009], we let

$$\sigma^2 = 1.09 \times 10^9 e^{1.26l}/(l+1)(2l+1)\,, \tag{5}$$

which is given as a function of the SH degree l. These series have lower time variability than the Gaussian processes of *Gillet et al.* [2009], where time constants are much shorter than 20 years. We point out, nevertheless, that our models and conclusions do not depend how the temporal variabilities of synthesized flows are prescribed, owing to the temporal smoothing implemented in the inversion. In this study, we generate 26 small-scale fields $B_r^{(k)}$ ($k = 1, \cdots, 26$) for a set of the four parameters L, p, λ_{TG}, and λ_p, to give statistics of the subsequent model such as ensemble average and standard deviation.

The time derivative $\dot{B}_r$ of radial field in (3) is supplied also by C^{3}FM2 SV up to SH degree 14. We exclude time derivatives of the synthesized field $\dot{B}_r^{(k)}$ as a constraint for small-scale SV, since we assess the SV misfit at the Earth's surface after upward continuation, where the small-scale signals may be too tiny to be observed robustly. For an estimate of the variance of C^{3}FM2 SV, we compare it with other SV models by calculating the RMS difference in all three field components at the Earth's surface. The weight W_l involved in $\mathcal{N}_{\mathrm{FF}}$ in (2) is given by referring to CM4 [*Sabaka et al.*, 2004]. More specifically, we let $W_l = (l+1)(2l+1)(V_l + D_l)^{-1}$, where V_l and D_l are our estimates of l-dependent SV variances in nT^2/yr^2 due to two different sources. V_l represents variances due to uncertainties of field modeling, given by the squared SV difference between C^{3}FM2 and CM4 for each l, averaged over the Earth's surface and the CM4 period 1960.0–2002.0. D_l is the variance due to uncertainty of magnetic diffusion, which we derive from B_r at the core surface by assuming "static diffusion" [*Holme and Olsen*, 2006; *Wardinski et al.*, 2008]. The values for these l-dependent variances are referred to in Table 1. The contribution of V_l to W_l is more important than that of D_l at every SH degree but $l = 3$ and 4.

In evaluating misfits of our flow models to C^{3}FM2 SV, we simply refer to a gross estimate of C^{3}FM2 SV variance, as often done in the flow inversions of historical magnetic field models constructed mostly from ground-based observatory data. At the Earth's surface, the RMS SV difference reads 8.2 nT/yr between C^{3}FM2 and CM4 for the period 1960.0–2002 and 7.0 nT/yr between C^{3}FM2 and "frozen-flux" C^{3}FM2 for 1957.0–2008.0 [*Wardinski and Lesur*, 2012]. Based on these estimates, we set ∼5.5 nT/yr as our reference value for the RMS misfit $\langle \Delta\dot{B} \rangle$ to C^{3}FM2 SV. Hereafter, we describe flow models with this reference misfit as *moderate fitting*.

Table 1. Estimates of the Observation Variance V_l and Diffusional Variance D_l for C^{3}FM2 SV in nT^2/yr^2 as a Function of SH Degree l

l	V_l	D_l	l	V_l	D_l	l	V_l	D_l	l	V_l	D_l
1	5.23	3.01	5	9.21	7.24	9	2.23	0.67	13	0.5	0.03
2	9.61	4.48	6	5.20	3.40	10	1.82	0.19	14	0.5	0.01
3	10.31	14.98	7	5.05	2.38	11	1.22	0.08			
4	9.56	13.52	8	2.86	0.73	12	0.5	0.04			

Let us make a remark on the alternative source of SV variance, which is due to underparametrizations of the magnetic field B_r and flow $\vec{u}_H$ in (3) [*Hulot et al.*, 1992]. The interaction of the truncated field and flow also produces large-scale SV, which leads to modeling error. Depending on their powers, the estimate of observational (or diffusional) variance may no longer be the primary source of SV variance [*Eymin and Hulot*, 2005; *Pais and Jault*, 2008]. In order to allow for the influence of possibly predominant modeling error on the CAM estimates, it is important to check how the estimated CAM variations vary with the SV misfit growing beyond the reference value defined above.

4. Results

The CAM variations are computed from diverse flow models built by changing the four inversion parameters L, p, λ_{TG}, and λ_p. For a smart systematic analysis, we search the ranges of these parameters in two steps: TG-fixed inversions and L-fixed inversions (Table 2). In the TG-fixed inversions, we vary L and p, while λ_{TG} is fixed at a large enough value to ensure rigorous compliance to the TG constraint. For each set of L and p, a flow solution is derived by adjusting λ_p to let it have a misfit $\langle \Delta \dot{B} \rangle$ to C^{3}FM2 SV that is moderate fitting. Our flow models derived in the TG-fixed inversions are listed in Table 3. In the L-fixed inversions, we vary p and λ_{TG} while L is fixed at 27. The field B_r is not supplemented by synthetic small-scale field $B_r^{(k)}$ in this second step. Some of our flow models derived in the L-fixed inversions are listed in Table 4.

All our models in Tables 3 and 4 are named [TG or TM]$L^{[\text{null or } (k)]}p^{[\text{null or } *]}$, where TG and TM indicate that λ_{TG} is greater and smaller than 3.0×10^1, respectively. We attach a superscript $*$ to the model names a posteriori, if their CAM trends appear to agree with the trend of LOD observation Λ_o. The superscript $^{(k)}$ indicates the use of core surface radial field B_r including the randomly synthesized small-scale component $B_r^{(k)}$ (see section 2.2). For an illustrative purpose, properties or behaviors of the models with $^{(k)}$ are represented by ensemble averages of the individual inversion solutions for $k = 1$ to 26.

4.1. Trend of Magnetically Estimated CAM Variations

4.1.1. Varying the Flow Truncation Degree

First, we present the LOD predictions Λ_J associated with our flow models estimated in the TG-fixed inversions (Table 3). In Figure 1, we plot Λ_J from TG14−1.0, TG14+0.0 and TG14+1.0, as well as the ensemble averages of $\Lambda_J^{(k)}$ ($k = 1, \cdots, 26$) for $L > 14$. These ensemble averages represent well the trends of individual LOD predictions $\Lambda_J^{(k)}$ that are not so dispersed because of the effective temporal damping. The plots reveal that there are TG flow models whose associated CAM variations have trends consistent with the observed LOD. Such models are only among those estimated with $p = -1.0$ (Figure 1); the trend is still too steep for $L = 14$, but larger L enhances the similarity between predicted and observed LOD trends. They agree well when $L \geqslant 20$. All the CAM trends with $p = 0.0$ and larger are obviously inconsistent with the LOD observation.

Table 2. Systematic Changes of the Parameters in the (i) TG-Fixed and (ii) L-Fixed Flow Inversions[a]

Parameter	L	p	λ_p	λ_{TG}
(i)	14, 20, 26, 32, 37	−1.0, 0.0, 1.0	Adjusted $\langle \Delta \dot{B} \rangle \simeq 5.5$ nT/yr (see Table 3)	10^5 (Fixed)
(ii)	27 (Fixed)	−1.0, −0.5, 0.0, 1.0	$10^{-3} \rightarrow 10^1$	$10^0 \rightarrow 10^3$

[a]The radial magnetic field $B_r (= \overline{B_r} + B_r^{(k)})$ at the CMB is truncated at SH degree L in (i) and 14 in (ii). See section 2.1 for the notations.

Table 3. List of Core Flow Models in the TG-Fixed Inversions[a]

Model	L	p	λ_p	λ_{TG}	$\langle u_H \rangle$		$\langle \Delta \dot{B} \rangle$		Type
TG14−1.0	14	−1.0	1.0×10^{-1}	1.0×10^{5}	16.87		5.64		–
TG20$^{(k)}$−1.0*	20	−1.0	2.6×10^{-1}	1.0×10^{5}	12.87	(0.16)	5.51	(0.24)	III
TG26$^{(k)}$−1.0*	26	−1.0	3.6×10^{-1}	1.0×10^{5}	11.62	(0.11)	5.42	(0.22)	III
TG32$^{(k)}$−1.0*	32	−1.0	4.2×10^{-1}	1.0×10^{5}	11.01	(0.12)	5.35	(0.26)	III
TG37$^{(k)}$−1.0*	37	−1.0	4.8×10^{-1}	1.0×10^{5}	10.52	(0.08)	5.38	(0.24)	III
TG14 + 0.0	14	0.0	1.0×10^{-2}	1.0×10^{5}	17.41		5.63		I
TG20$^{(k)}$+0.0	20	0.0	2.3×10^{-2}	1.0×10^{5}	13.84	(0.12)	5.50	(0.22)	I
TG26$^{(k)}$+0.0	26	0.0	3.1×10^{-2}	1.0×10^{5}	12.73	(0.11)	5.54	(0.25)	I
TG32$^{(k)}$+0.0	32	0.0	3.6×10^{-2}	1.0×10^{5}	12.19	(0.13)	5.57	(0.20)	I
TG37$^{(k)}$+0.0	37	0.0	4.0×10^{-2}	1.0×10^{5}	11.81	(0.08)	5.60	(0.12)	I
TG14+1.0	14	1.0	1.0×10^{-3}	1.0×10^{5}	17.89		5.71		I
TG20$^{(k)}$+1.0	20	1.0	2.0×10^{-3}	1.0×10^{5}	14.94	(0.19)	5.63	(0.18)	I
TG26$^{(k)}$+1.0	26	1.0	2.5×10^{-3}	1.0×10^{5}	14.18	(0.14)	5.59	(0.16)	I
TG32$^{(k)}$+1.0	32	1.0	2.6×10^{-3}	1.0×10^{5}	13.97	(0.16)	5.48	(0.16)	I
TG37$^{(k)}$+1.0	37	1.0	2.7×10^{-3}	1.0×10^{5}	13.80	(0.10)	5.43	(0.15)	I

[a] $\langle u_H \rangle$ denotes the RMS flow velocity in km/yr and $\langle \Delta \dot{B} \rangle$ the RMS misfit to C^{3}FM2 in nT/yr. Ensemble averages and standard deviations (parentheses) are given for the models estimated using synthesized $B_r^{(k)}$. The definition of "Type" is referred to in the main text of section 3.1.

The power spectra of the flow models, involving both the toroidal and poloidal flows altogether, are displayed in Figure 2. For $L > 14$, the plotted spectra are the ensemble averages of those of the 26 individual solutions, which are very similar to one another, particularly at lower SH degrees. Notably, the spectrum for $p = -1.0$ alone exhibits a distinct behavior. The large-scale flows are damped relatively effectively by the power law constraint. The powers at SH degrees 1 to 5 are even lower than around 10 to 14, indicating that these models are "intermediate-scale TG flow models." We note that the powers at SH degree 1 are no larger than 6 km^2/yr^2 for TG20$^{(k)}$−1.0*, TG26$^{(k)}$−1.0*, TG32$^{(k)}$−1.0*, and TG37$^{(k)}$−1.0*. For TG14-1.0, however, a significantly larger power is required at SH degree 1 (as well as the whole flow velocity $\langle u_H \rangle$ (Table 3)), which makes the associated CAM trend disagree with the observed LOD trend. Much in the same way, all the models for $p = 0.0$ and 1.0 fail to have the favorable CAM trend, as they have as much power as $\sim$ 20 km^2/yr^2 at the lowest SH degree. These models are "large-scale TG flow models," whose spectra monotonically decay with SH degree (except for TG14+0.0 and TG14+1.0).

4.1.2. Relaxing the TG Constraint

The results of the L-fixed inversions indicate that many differing flow models can agree with the observed LOD trend, once the TG constraint is relaxed. In order to quantify the similarity in the observed and predicted LOD trends, we introduce the RMS difference

$$\Delta \dot{\Lambda} = \left\langle \dot{\Lambda}_o - \dot{\Lambda}_J \right\rangle \tag{6}$$

Table 4. List of Core Flow Models in the L-Fixed Inversions[a]

Model	L	p	λ_p	λ_{TG}	$\langle u_H \rangle$	$\langle \Delta \dot{B} \rangle$	$\sigma_{\dot{B}}^{(B^<)}$	Type
TG27+1.0	27	1.0	1.8×10^{-3}	1.0×10^{3}	15.48	5.52	9.14	I
TM27−1.0	27	−1.0	1.5×10^{0}	1.0×10^{0}	6.05	5.51	5.12	II
TG27−1.0*	27	−1.0	4.0×10^{-1}	6.3×10^{1}	10.91	5.67	10.53	III
TM27−0.5*	27	−0.5	3.2×10^{-1}	1.3×10^{1}	7.75	5.73	4.33	IV
TM27+0.0*	27	0.0	1.6×10^{-1}	7.9×10^{0}	8.00	5.55	2.83	IV
TM27+1.0*	27	1.0	2.5×10^{-2}	5.0×10^{0}	9.51	5.30	1.97	IV

[a] See the legend of Table 3 for the notations. $\sigma_{\dot{B}}^{(B^<)}$ stands for the standard deviation of the SV prediction $\langle \Delta \dot{B} \rangle$ due to the uncertainty of truncated magnetic field, computed from the assumed variance σ^2 (5) for SH degrees $15 \le l \le 27$.

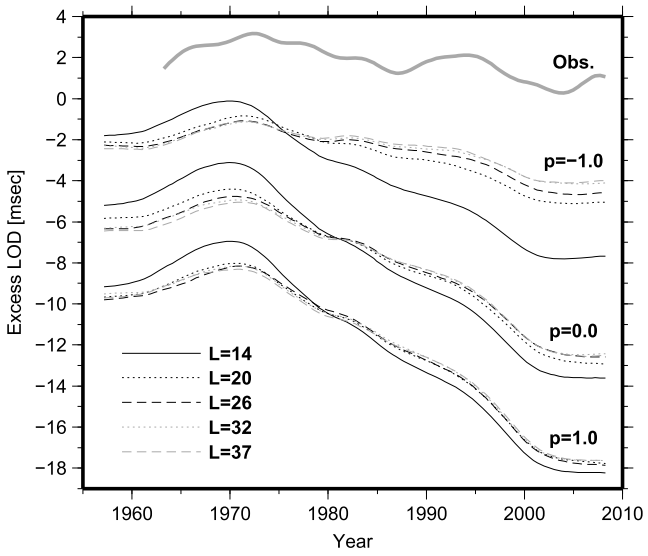

Figure 1. The observed excess LOD Λ_o and the predictions from the CAM variations Λ_J computed with *Jackson*'s [1997] formula (1). Plotted are Λ_J from TG14−1.0, TG14+0.0, and TG14+1.0, as well as the ensemble averages of 26 predictions $\Lambda_J^{(k)}$ ($k = 1, \cdots, 26$) for each combination of L (= 20, 26, 32 and 37) and p (= −1.0, 0.0 and 1.0) (see also Table 3). For an illustrative reason, the predictions for $p = 0.0$ and 1.0 are shifted vertically by −3 and −7 ms, respectively.

between time derivatives of the LOD observation $\dot{\Lambda}_o$ and prediction $\dot{\Lambda}_J$, where the bracket stands for the RMS over the model time period. In Figure 3, $\Delta\dot{\Lambda}$ is plotted as a function of λ_{TG} and λ_p, and with respect to four values of $p = -1.0, -0.5, 0.0$, and 1.0. The plot for each p is based on 1200 L-fixed inversions, for which λ_{TG} and λ_p are evenly sampled within their parameter range (see Table 2). The isolines of RMS SV misfit $\langle \Delta\dot{B} \rangle$ at 5.5 nT/yr are also overlaid, which delineate availability of a moderate fitting model for any choice of λ_{TG}. The values of λ_p along these isolines vary most rapidly within the range of λ_{TG} between 10^1 and 10^2 for all p. This is indeed the transition range between TG dominance (for $\lambda_{TG} \gtrsim 3\times10^1$) and TM dominance (for $\lambda_{TG} \lesssim 3\times10^1$).

$\Delta\dot{\Lambda}$ reaches a minimum value along the isolines of reference misfit 5.5 nT/yr for all p in Figure 3. This is due to the general tendency of the estimated CAM: their trends (and the subsequent Λ_J trends) are gradually steepened as the TG constraint is tightened. The 5.5 nT/yr isolines are thus divided by the $\Delta\dot{\Lambda}$ minima into where the Λ_J trends are steeper and less steep than the observed LOD trend (toward larger and smaller λ_{TG}, respectively). Among the moderate fitting models estimated with an equal value of λ_{TG}, the CAM trend steepens as p increases from −1.0 to 1.0. The position of $\Delta\dot{\Lambda}$ minima along the isolines is thus shifted toward the TG-dominant domain as p decreases from 1.0 to −1.0.

To illustrate this in more detail, we pick six moderate fitting models from the L-fixed inversions, which are listed in Table 4. Four of them, TM27+1.0*, TM27+0.0*, TM27−0.5*, and TG27−1.0*, which are all at the vicinities of the minima of $\Delta\dot{\Lambda}$ along the 5.5 nT/yr isolines (purple stars in Figure 3), actually have CAM trends consistent with the observed LOD trend (Figure 4). Toward larger λ_{TG}, the resulting CAM trends become steeper. This effect is of particular significance for large-scale models ($p \geq 0.0$), as is the case with TG27+1.0 (orange star in Figure3d and grey solid line in Figure 4) and those obtained in the TG-fixed inversions with $p \geq 0.0$ (Figure 1). This confirms systematically the previous findings with large-scale flow models [*Wardinski*, 2005; *Gillet et al.*, 2009], emphasizing a strong tendency for large-scale TG flow models to yield steep CAM trends. Toward smaller λ_{TG}, the resulting CAM trends flatten, especially for intermediate-scale models ($p = -1.0$) such as TM27−1.0 (orange star in Figure3a and grey dashed line in Figure 4).

From a dynamical consideration (see section 4.2), we classify our moderate fitting models agreeing with the observed LOD trend. The first group is formed by TG-dominant models, such as TG27−1.0* and those obtained in the TG-fixed inversions with $p = -1.0$ and $L \geq 20$. The second group consists of TM-dominant models derived with $p = 0.0$ and 1.0, e.g., TM27+0.0* and TM27+1.0*. There are some models in between that are not clearly discriminated, such as TM27−0.5*, which we here include in the second group.

The results of the systematic analysis suggest that our flow models may be sorted out into four main types (see also Tables 3 and 4): (I) large-scale TG flow with its CAM trend being too steep, (II) intermediate-scale TM

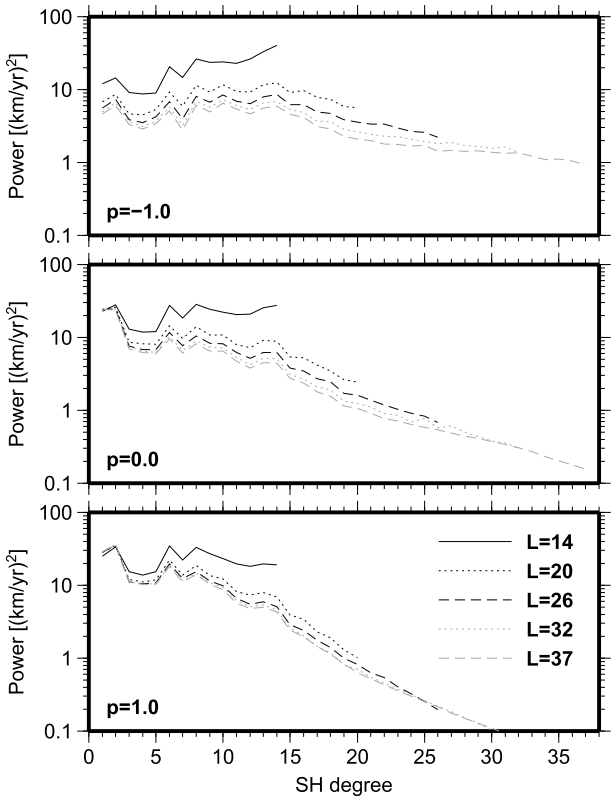

Figure 2. The power spectra of flow models at 2000.0, involving both toroidal and poloidal flow contributions. The models are estimated with varying values of p and L in the TG-fixed inversions. The plotted spectra for $L = 20$ and larger are the ensemble averages of 26 individual spectra for each set of L and p.

flow with its CAM trend being too flat, and (III) intermediate-scale TG flow and (IV) large-scale TM flow with their CAM trends consistent with the observed LOD trend.

The spatial flow patterns differ significantly among moderate fitting models of the different types. Type (I) has features in common with previous TG flow models, noticeably including the equatorially symmetric retrograde vortices in the Atlantic hemisphere (Figure 5a). It has pronounced westward zonal jets with a remarkable growth during the 30 years following 1970.0 (Figure 6a), particularly around 30°S, where the Taylor cylinders have a relatively large moment of inertia. Such equatorial jets are actually least present in Type (II) (Figure 6b) leading to an inadequate CAM trend. Type (III) and Type (IV) rather contrast with each other, although they both are compatible with the observed LOD trend. Type (III) have relatively weak westward winds (Figure 6c) and many eddy flows (Figure 5c) in the midlatitudes, while Type (IV) contains westward winds in abundance (Figures 6e and 6f), their temporal evolutions being nevertheless not as much as those of Type (I) (Figure 6a).

4.2. Rapid CAM Variations

We investigate time derivatives of the CAM estimates to identify rapid CAM variations better, as their amplitude may be smaller by an order of magnitude than the decadal components (Wardinski and Asari, submitted manuscript, 2015). We present the results of analyzing the time derivative of LOD prediction $\dot{\Lambda}_J$ in the time domain.

4.2.1. Correlations Among Varying Models

In Figure 7 we plot $\dot{\Lambda}_J$ for the two moderate fitting models from L-fixed inversions, TG27−1.0* and TM27+1.0*, introduced in the previous subsection (Table 4). Their peaks and dips in $\dot{\Lambda}_J$ occur at the same epochs, despite the contrasting characteristics of these models in the physical background, spectra, and spatial flow patterns. The phase coherency in $\dot{\Lambda}_J$ is also true for other moderate fitting models in the L-fixed inversions. Moreover, the concurrences are obviously seen for the models with both overfitting and underfitting models (also shown in Figure 7). The coherency is robust even when a larger SV misfit is allowed to accommodate modeling error due to truncated field and flow. These results suggest that the phase of estimated CAM variation, including its subdecadal components, is not determined as a result of the TG constraint or the regularization.

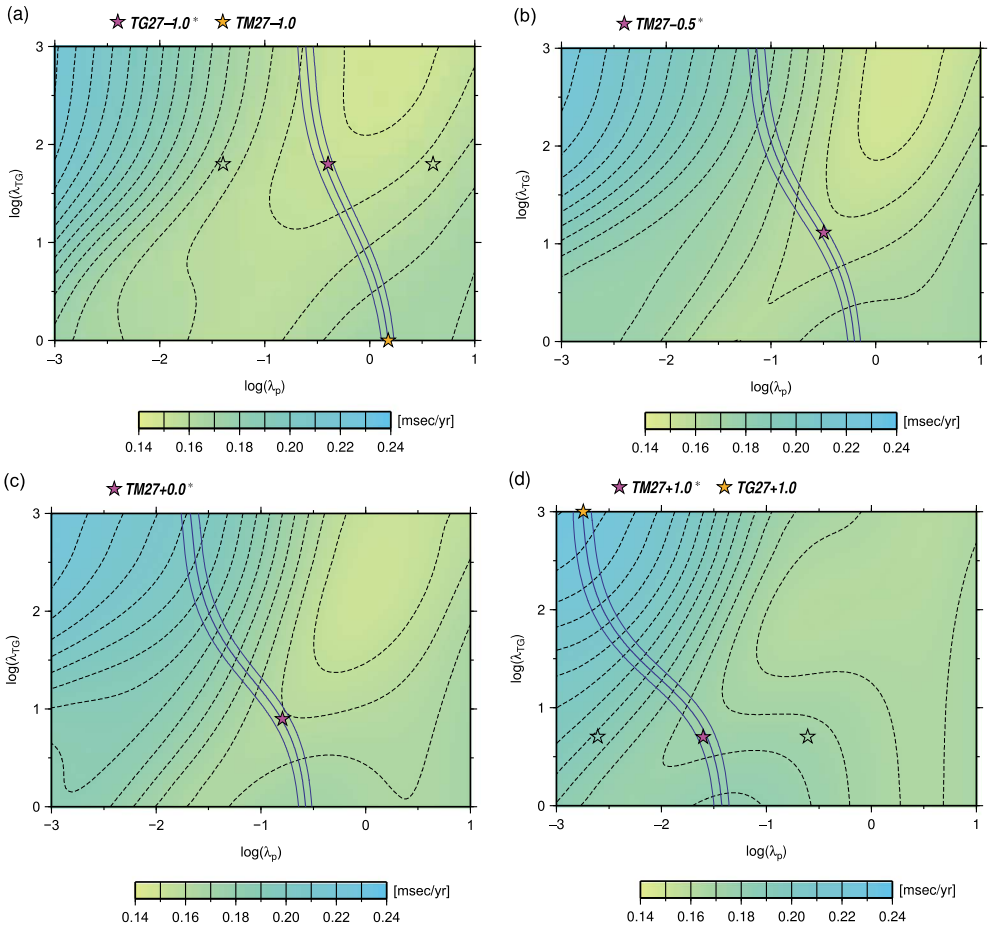

Figure 3. $\Delta\dot{\Lambda}$ (color scale and dashed line contours with intervals of 0.005 ms/yr) defined by (6) derived in the systematic inversions with $L = 27$. The quantity is plotted as a function of λ_{TG} and λ_p, for (a) $p = -1.0$, (b) $p = -0.5$, (c) $p = 0.0$, and (d) $p = 1.0$. Also plotted are contours of the RMS SV misfit $\langle \Delta\dot{B} \rangle$ to C^{3}FM2 SV at 5.5 nT/yr (thick blue curve), as well as 5.0 (thin blue curve to the left) and 6.0 nT/yr (thin blue curve to the right). The six models obtained in the *L*-fixed inversions are also plotted with colored stars. The open stars in Figures 3a and 3d signify the overfitting (to the left) and underfitting models (to the right) presented in section 4.2.1 and Figure 7.

The phase of subdecadal $\dot{\Lambda}_J$ fluctuations are fundamentally not altered by selecting physical constraints other than the TG and TM constraints. In Figure 8, we plot $\dot{\Lambda}_J$ associated with flow models under various constraints, alongside the TG and TM ones. In addition to the commonly used constraints of the purely toroidal flow and helical flow [*Holme*, 2007], they include the constraints of the anisotropy flow [*Schaeffer and Pais*, 2011] and the quasi-geostrophy flow [*Pais and Jault*, 2008]. The phase coherency is still seen among the rapid $\dot{\Lambda}_J$ fluctuations of these models (except for some peculiarity in the helical flow model).

It follows that the phase of $\dot{\Lambda}_J$ originates intrinsically in the input magnetic field model. Interestingly, the phase of subdecadal fluctuation of $\dot{\Lambda}_J$ is almost unchanged even for flows estimated only from the large-scale components of C^{3}FM2 (Figure 9). This means that the typical phases of decadal and subdecadal variations of $\dot{\Lambda}_J$ are effectively constrained by large-scale MF and SV alone (more specifically by those up to SH degree 4, according to Figure 9).

There appears to be a positive correlation between the estimation $\dot{\Lambda}_J$ and observation $\dot{\Lambda}_o$ as well. The correspondences of their peaks and dips are recognizable in either Figure 7 or 9, if not strictly concurrent. Aside from the minor lags, the rapid fluctuations of $\dot{\Lambda}_J$ and $\dot{\Lambda}_o$ are roughly in phase, while the amplitude is always significantly smaller for $\dot{\Lambda}_J$ than for $\dot{\Lambda}_o$. The amplitude of $\dot{\Lambda}_J$ is subject to a large uncertainty, however, as can be seen in Figures 7–9.

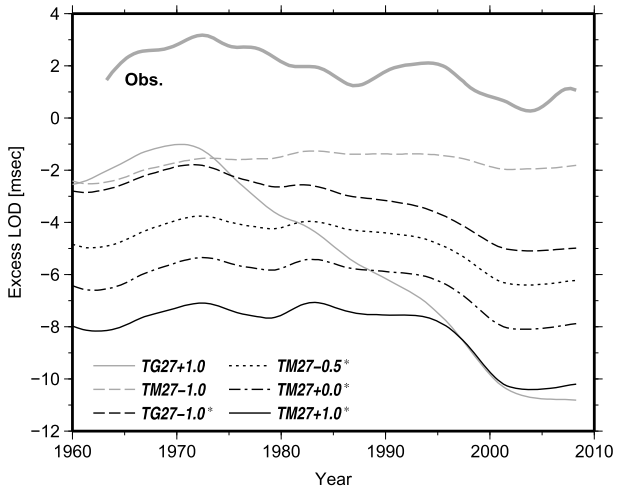

Figure 4. The observed excess LOD Λ_o and the predictions Λ_J (equation (1)) from the six flow models obtained in the *L*-fixed inversions and listed in Table 4.

4.2.2. Uncertainty of the Rapid CAM Variations

While the phase of $\dot{\Lambda}_J$ is determined coherently by the extensively different flow models derived from C^{3}FM2, it is yet to be conclusive that the phase of Earth's 6 year CAM oscillation is detected robustly by magnetic observations. Allowance should be made for its potential uncertainty if it would be applied to discussion of the Earth phenomena. For the observational uncertainty we refer to Wardinski and Asari (submitted manuscript, 2015), where estimates of $\dot{\Lambda}_J$ phase do not agree between those based on the two magnetic models, C^{3}FM2 and FF-C^{3}FM2, constructed from the same data set. As remaining sources of uncertainty, we consider the dispersion of $\dot{\Lambda}_J$ due to the synthesized small-scale field $B_r^{(k)}$ and the ignorance of CAM variation due to the incomplete resolution.

Effects of the synthesized small-scale field $B_r^{(k)}$ on rapid components of the CAM estimation are displayed in Figure 10, where we plot $\dot{\Lambda}_J^{(k)}$ from the individual flow solutions ($k = 1, \cdots, 6$) that have been used to derive the statistics of TG20$^{(k)}$+1.0, TG37$^{(k)}$+1.0, TG20$^{(k)}$−1.0*, and TG37$^{(k)}$−1.0*. In all these four settings, the rapid behaviors of $\dot{\Lambda}_J^{(k)}$ are not clearly correlated with one another (accordingly, rapid variations are poorly seen in their ensemble averages (Figure 1)) nor with those of the time derivative of observed LOD $\dot{\Lambda}_o$. Imaging of subdecadal variations of the largest-scale flows can be affected by accounting for the temporally varying $B_r^{(k)}$. Meanwhile, the decadal variations of $\dot{\Lambda}_J^{(k)}$ are correlated among themselves and even with $\dot{\Lambda}_o$ (Figure 10), as signified by their common peaks in late 1960s, early 1980s, early 1990s, and late 2000s, as well as their dips in middle 1970s and late 1990s.

A resolution test is also performed with the settings of the *L*-fixed inversions (where $B_r^{(k)}$ is absent). Resolution of an inversely estimated flow model may usually be evaluated by referring to the resolution matrix [e.g., *Wardinski et al.*, 2008; *Asari and Lesur*, 2011]. The test here is more straightforward. Following the modeling approach by *Holme* [1998], we prepare flow models such that their CAM variations may perfectly explain the observed LOD time derivative $\dot{\Lambda}_o$. These models are estimated from C^{3}FM2 with the same inversion parameters as in Table 4. They are still moderate fitting. We refer to these models as "virtual core." Now taking a virtual core as the target to resolve, we again invert its SV prediction—exclusively up to SH degree 14—to check whether the CAM variation of virtual core is retrieved. Here the recovered flow is moderate fitting to the virtual core, only λ_p being modulated, and p, L, and λ_{TG} remaining the same as in Table 4.

Figure 11 shows the results of the resolution test performed with the same inversion settings as used for the C^{3}FM2 flow models TM27−1.0, TG27+1.0, TG27−1.0*, and TM27+1.0* (Table 4). None of the recovered CAM variations are found entirely faithful to the original CAM behavior of the virtual core which perfectly explains $\dot{\Lambda}_o$. They are rather close to the CAM variations of the C^{3}FM2 flow models. There arises a concern that even the coherently determined phase of subdecadal variations of $\dot{\Lambda}_J$ (section 4.2.1) may not well represent that of the Earth's CAM variation.

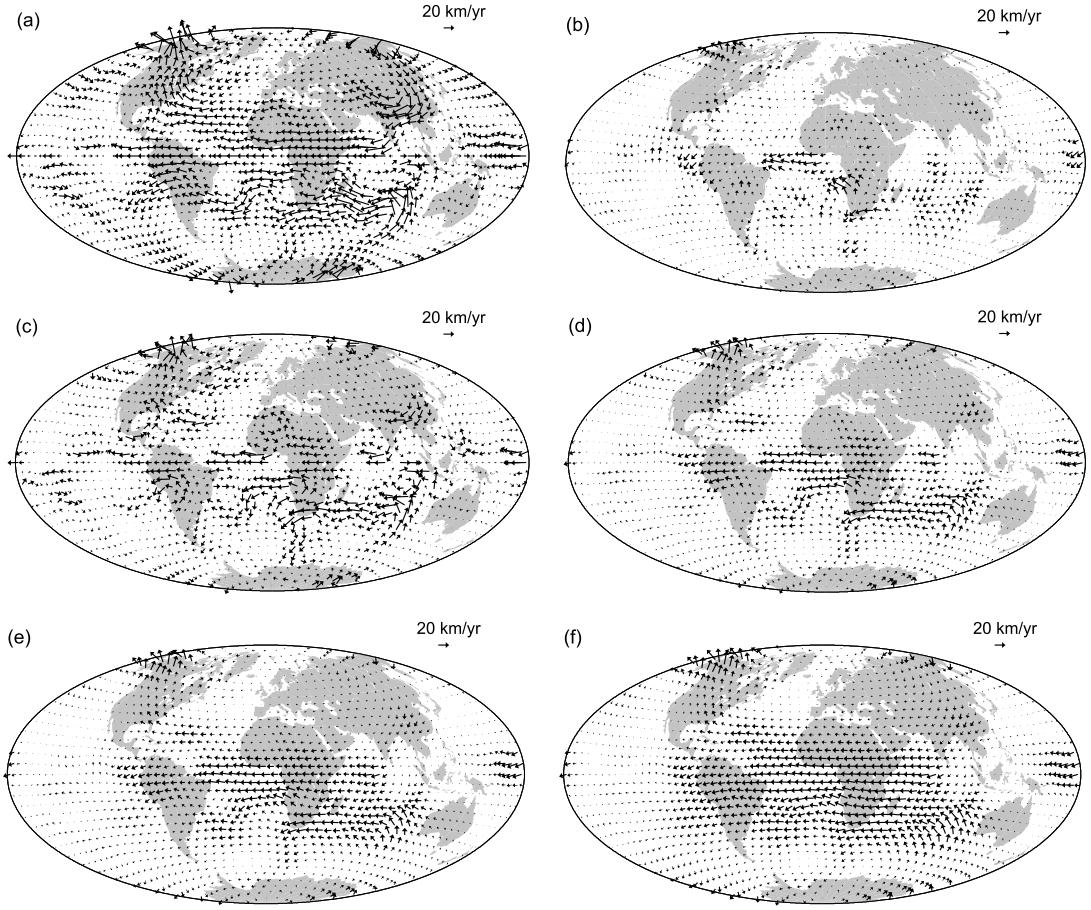

Figure 5. The flow maps at 2000.0 for the six models obtained in the *L*-fixed inversions: (a) TG27+1.0, (b) TM27−1.0, (c) TG27−1.0*, (d) TM27−0.5*, (e) TM27+0.0*, and (f) TM27+1.0*.

5. Discussion

5.1. Implications on the Core Flow Inversion From the Estimates of CAM Trend

A general tendency for the estimated CAM trends can be induced from our analysis based on the systematic core flow inversions. For a certain fixed SV misfit, the trend steepens as the degree of freedom allowed to the flow diminishes. This happens, for instance, when small-scale flow components are more strongly damped (with increasing p) or truncated at a lower SH degree (with decreasing L) or a tighter physical constraint is imposed (with increasing λ_{TG}). Tightly constrained flow models are apt to rely on a relatively intense zonal toroidal flow to account for the SV, which leads eventually to an excessively steep trend of estimated CAM variation. This kind of flow pattern tends to be pronounced particularly in TG flow models. Once TG is relaxed into a weaker constraint of TM, the circumstances are alleviated, in which the requirements on the other factors, small-scale flow damping, truncation, or SV misfit, are less strict. In analogy, an enhancement of zonal toroidal flow variation is expected among flow models that are derived, for example, with $p = 3$, equivalent to the strong norm of *Bloxham* [1988].

It is worth emphasizing that the CAM trend can still be consistent with the observed LOD trend even under the strong constraint of rigorous TG. As is the case with intermediate-scale TG flow (Type (III)) models, e.g., TG37$^{(k)}$−1.0*, the intense zonal circulation is absent and small-scale advections play a certain role in generating the large-scale SV. This implies in turn that the emergence of intense global circulation in large-scale TG flow (Type (I)) models may be interpreted as an effect of aliasing as a consequence of underparametrization or excessive spatial smoothing. This process is well illustrated in an inversion test by *Rau et al.* [2000], where a large-scale TG flow inversion is performed in an attempt of recovering an intermediate-scale numerical dynamo flow.

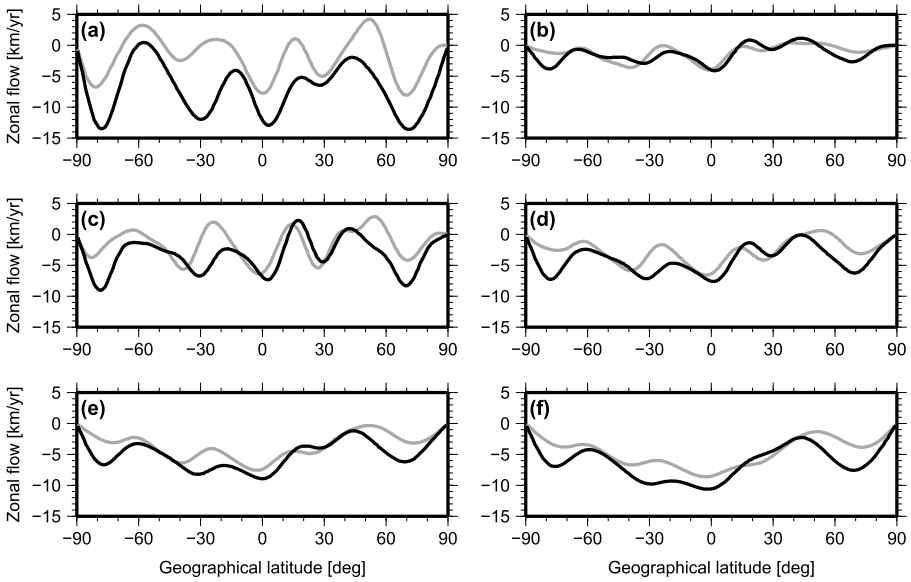

Figure 6. Zonal toroidal flow velocities as a function of the geographical latitude at 1970.0 (gray) and 2000.0 (black), for six models obtained in the *L*-fixed inversions: (a) TG27+1.0, (b) TM27−1.0, (c) TG27−1.0*, (d) TM27−0.5*, (e) TM27+0.0*, and (f) TM27+1.0*.

The above argument on the tendency of estimated CAM trend applies also to some of previous works using flow models obtained with different constraints. The centennial flow models by *Pais et al.* [2004] have too flat a trend for the period of our current interest, be it TG or non-TG (in their context), perhaps because these models have quite low powers for flows at largest scales, as is the case with TM27−1.0. Also in the CAM estimations from a satellite magnetic field model GRIMM2 for 2000.0 to 2010.0 [*Lesur et al.*, 2008], we see the variation which is steeper for their TG model than TM model [*Asari and Lesur*, 2011]. The quasi-geostrophy constraint used by *Gillet et al.* [2009] is even more effective in reducing the flow space than TG, so a steep CAM trend is expected, as is the case with their actual CAM estimation. Subject to the strong constraint of equatorial symmetry, nevertheless, the trend steepness is eased by regularizing the inversion with the anisotropy flow assumption, whereby the flow is smoothed preferentially in the azimuthal direction [*Schaeffer and Pais*, 2011]. This may be owing to their regularization which is relatively ineffective in reducing the flow degree of freedom.

Another tendency to be noted is that intermediate-scale TG flow (Type (III)) models remain compatible with the observed LOD trend when a larger SV misfit is allowed. The tendency can be seen in Figure 3, where the SV misfit grows with increasing λ_p and λ_{TG} along the trough line of $\Delta\dot{\Lambda}$. This proves in favor of Type (III) models, in that their compatibility with the observed LOD trend is still assured even when the modeling error dominates the observation error. Note that considering the modeling error, Type (III) models intrinsically require larger SV misfits than the large-scale TM flow (Type (IV)) models. In Table 4, we add the modeling errors, for reference, in the form of SV standard deviations $\sigma_{\dot{B}}^{(B^<)}$ over the Earth's surface. These are calculated from the magnetic field variance σ^2 extrapolated for truncated field (5), by applying the linear propagation of Gaussian variance to the induction equation (3) for each model of the flow $\vec{u}_H$. For all the TM models in Table 4, $\sigma_{\dot{B}}^{(B^<)}$ are smaller than the reference misfit 5.5 nT/yr. However, this is not the case with the TG models TG27−1.0* and TG27+1.0, indicating a need of some larger SV misfit for those models to be consistent with the modeling error. Unless smoothed even more effectively, e.g., with $p = 3$, no TG model would be available that is simultaneously moderate fitting and not affected by the modeling error (see also *Celaya and Wahr* [1996] and *Holme and Olsen* [2006] on this issue). In view of the tendency discovered here, nevertheless, we still do not find any disadvantages of Type (III) over Type (IV) in agreeing with the observed LOD trend.

5.2. Insights on the Core Dynamics From the Estimates of CAM Trend

The two contrasting flow types that are found favored by the observed LOD trend, i.e., Type (III) and Type (IV) (Table 4), apparently correspond to two characteristic regimes of spherical shell dynamo in numerical simulations. Various settings tested by *Hori et al.* [2012] include dynamos powered exclusively by a buoyancy source at the inner boundary, which could possibly be models for the geodynamo. The flows in those

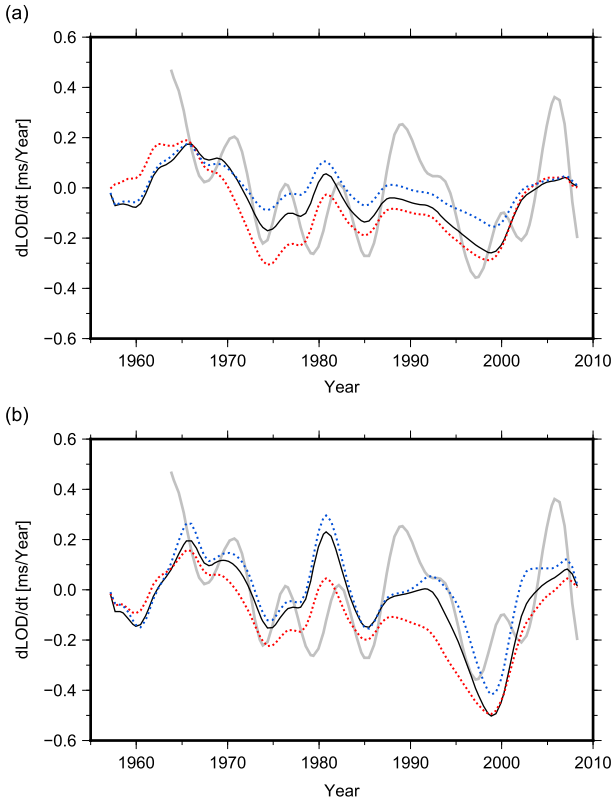

Figure 7. Time derivatives $\dot{\Lambda}_J$ of LOD predicted from the flow models (a) TG27−1.0* and (b) TM27+1.0* (black solid). $\dot{\Lambda}_J$ from the overfitting models (red dotted) and underfitting models (blue dotted) are also plotted in each panel (the former and latter are obtained respectively by increasing and decreasing λ_p by an order of magnitude; see Figures 3a and 3d). The SV misfits $\langle \Delta \dot{B} \rangle$ of the overfitting models are (a) 2.05 and (b) 2.23 nT/yr and of the underfitting models (a) 17.32 and (b) 15.63 nT/yr. The time derivative $\dot{\Lambda}_o$ of the observed LOD is shown as well (grey solid).

runs have a predominant scale in space, which vary with how the thermochemical boundary conditions are defined at the inner and outer boundaries, selected from either condition of fixed codensity or fixed codensity flux. The case with fixed codensities at both boundaries (BS-CC in *Hori et al.* [2012]), alongside many other dynamos under the similar condition [e.g., *Christensen et al.*, 1999; *Sreenivasan and Jones*, 2006], does not promote planetary-scale flows, with its kinetic energy peaking around SH order 10. Generally, such dynamos are of α^2 type, where magnetic field intensity is as large in the bulk of the fluid region as at the outer surface and the primary force balance is geostrophic. These features are shared by our Type (III) models. Meanwhile, the

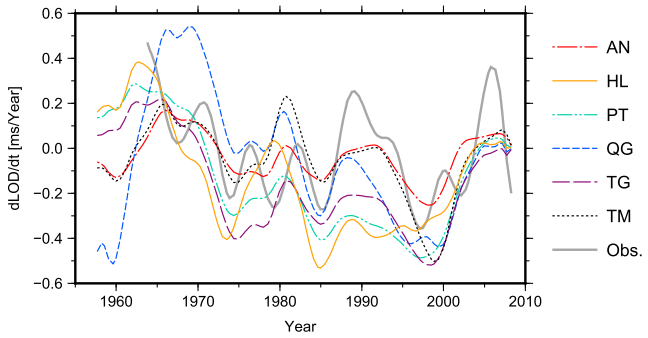

Figure 8. Time derivative of the LOD observation $\dot{\Lambda}_o$ (Obs.) and those of the predictions $\dot{\Lambda}_J$ according to flow models estimated from C^{3}FM2 (without the synthesized field $B_r^{(k)}$) under different physical assumptions: anisotropy flow (AN), helical flow (HL), purely toroidal flow (PT), and quasi-geostrophy flow (QG). All these models are estimated with $(L, p) = (27, 1.0)$ and are moderate fitting except for the QG model for which $\langle \Delta \dot{B} \rangle = 19.0$ nT/yr. Also plotted are $\dot{\Lambda}_J$ for (TG) TG27+1.0 and (TM) TM27+1.0* (Table 4).

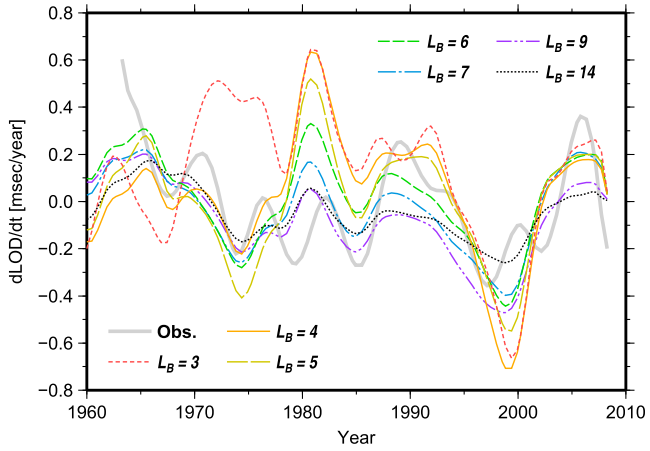

Figure 9. Time derivative of the LOD observation $\dot{\Lambda}_o$ (thick light grey) and those of the predictions $\dot{\Lambda}_J$ according to TM core flow models estimated from C^{3}FM2 whose MF B_r and SV $\dot{B}_r$ (to be input in (3) and (4)) are both truncated at SH degrees $L_B = 3, 4, 5, 6, 7, 9$, and 14. The flow truncation degree is given by $L = 2L_B - 1$. All models are moderate fitting, derived with $p = -1$ and $\lambda_{TG} = 6.3 \times 10^1$. The model with $L_B = 14$ is identical to TG27−1.0* given in Table 3.

case with fixed codensity fluxes at both boundaries (BS-FF in *Hori et al.* [2012]) is dominated by planetary-scale flows, with its kinetic energy spectrum monotonically decreasing with SH order. The ω effect should play a certain role in this kind of dynamo, where the toroidal magnetic field is significantly larger than the poloidal field and the magnetostrophic force balance is also prevalent [*Sakuraba and Roberts*, 2009]. Our Type (IV) models have these features in common.

The two regimes remain eligible for the geodynamo, as long as referring to the consistency with the observed LOD trend during the recent 50 years. Unfortunately, no decisive clue is gleaned as to which is more plausible for the Earth's core. At least, we expect more difficulties in properly predicting the LOD trend, when constraints are used which are even stronger than TG, such as the strict equatorial symmetry based on the quasi-geostrophy or columnar flow assumption [*Amit and Pais*, 2013]. These difficulties are already seen in recent efforts of incorporating magnetic observation in numerical dynamo modeling by *Aubert* [2013]. Characterized by flow structures of columnar convection along the rotation axis of the system, all his

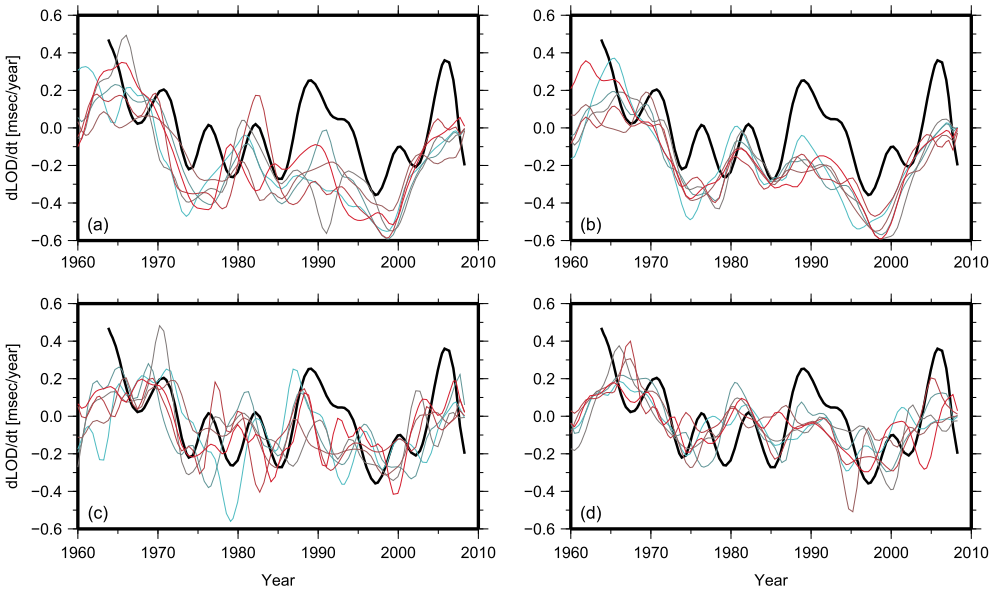

Figure 10. Time derivatives of the observed LOD $\dot{\Lambda}_o$ (thick black curve) and six predictions $\dot{\Lambda}_J^{(k)}$ $(k = 1, \cdots, 6)$ derived with variously synthesized small-scale field $B_r^{(k)}$ $(k = 1, \cdots, 6)$ (thin colored curves) for (a) TG20$^{(k)}$+1.0, (b) TG37$^{(k)}$+1.0, (c) TG20$^{(k)}$−1.0*, and (d) TG37$^{(k)}$−1.0* (Table 3).

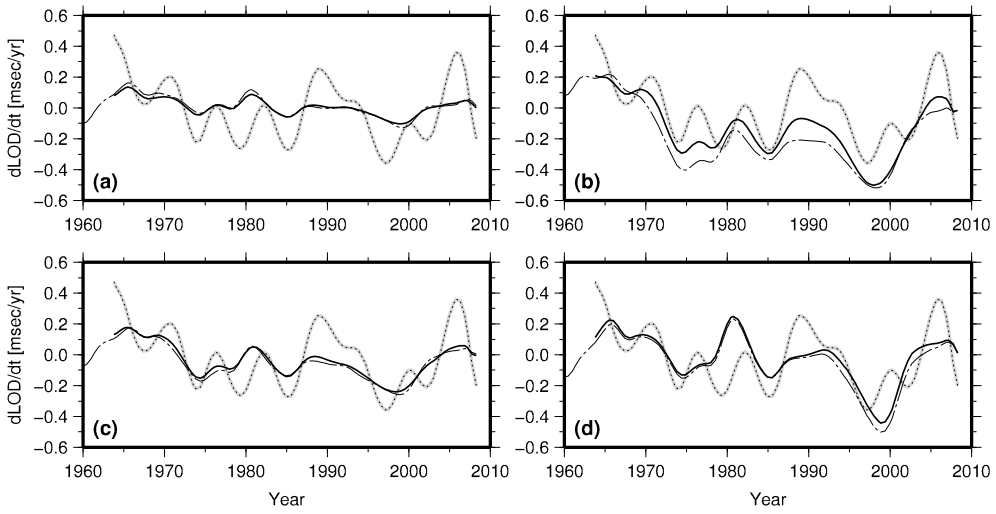

Figure 11. Time derivatives of the observed LOD $\dot{\Lambda}_o$ (thick grey line) and predictions $\dot{\Lambda}_J$ from the four C^{3}FM2 flow models (a) TM27−1.0, (b) TG27+1.0, (c) TG27−1.0*, and (d) TM27+1.0* (black dash-dotted line). Also plotted are $\dot{\Lambda}_J$ from the virtual core built with the same inversion parameters as used to derive the C^{3}FM2 flow models (black dotted line) and from the flow retrieved from the virtual core SV up to SH degree 14 (black solid line).

chemically driven dynamos, used as prior flow constraints in a statistical manner, hold a predominance of geostrophy, as well as equatorial symmetry, though not strict. The overall magnitude of azimuthal flows can be arbitrarily controlled by modifying efficiency of the gravitational locking between the internal and external shells. Model 2 of *Aubert* [2013], which is built from a prior dynamo without the gravitational boost of the azimuthal flow, accounts for CM4 and the observed LOD trend at the same time and apparently resembles our Type (III) models, with its kinetic energy spectrum peaking at SH degree 10. However, the very flow components carrying the angular momentum of whole fluid, composed notably of an intense global circulation typical of quasi-geostrophy models [*Pais and Jault*, 2008; *Gillet et al.*, 2009], fail to comply with the prior dynamo. On the other hand, Model 3 of *Aubert* [2013], which is built from a prior dynamo with enhanced azimuthal flows, accounts for CM4 and the prior dynamo, but its CAM trend turns out to be too steep.

5.3. Detecting Earth's 6 Year CAM Oscillation

We consider our systematic analysis of rapid CAM variations not yet sufficient for arguing that Earth's 6 year CAM oscillation is robustly resolved by magnetic observation. The results of the analysis give suggestions that are both in favor (section 4.2.1) and disfavor (section 4.2.2). Still finding a point in further pursuing the magnetic detection of the 6 year oscillation in Earth's core, we approach this with skepticism. Here we discuss multiple obstacles precluding the detection. The first two concern observation and modeling errors and have much to do with the principal difficulty lying in the subtleness of the relevant flow variations. The last, but not least, is the matter of theoretical limitation.

The first obstacle arises from the quality of historical magnetic field models. Core flow variations are resolved mainly by the secular acceleration [*Lesur et al.*, 2010]. It is already reported that some subdecadal periodicities in the observed secular acceleration are detected by a Fourier analysis [*Silva et al.*, 2012]. Subject to the low signal-to-noise ratio, however, these field periodicities would be hard to attribute firmly to CAM fluctuations, at least on the basis of C^{3}FM2 core flow modeling. The secular acceleration in the polar regions is even less certain due to the scarcity of observatories in addition to relatively large external field noise, although revealing the flow variation in these regions might help facilitate discussions on the role of gravitational inner core-mantle coupling. This problem may be brought down by employing a satellite field model that describes the core field with much higher precision in space and time. Thanks to the Swarm mission currently operating in succession to the Ørsted and CHAMP missions, the satellite observation era will cover three cycles of the 6 year LOD variation in the near future. Satellite field and flow models of this length will probably give a better opportunity to assess the magnetic detectability of the small CAM signals.

Second, the estimation of rapid CAM variations can be disturbed considerably by allowing for unknown small-scale magnetic field. Note that the rapid behavior in the estimated CAM (see Figure 10 for the time derivatives of the predicted LOD $\dot{\Lambda}_J^{(k)}$) is not directly determined by the synthesized small-scale field $B_r^{(k)}$, as

the interactions between $B_r^{(k)}$ and the largest-scale flows responsible for the CAM variation do not contribute to the large-scale SV, the most important part of SV at the Earth's surface. The rapid fluctuations of $\dot{\Lambda}_J^{(k)}$ are rather indirect outcomes of the fluctuating perturbation $B_r^{(k)}$ through the whole inversion process, which adds to the difficulty of identifying the 6 year CAM variation. It could be, nevertheless, that the random perturbations of $\dot{\Lambda}_J^{(k)}$ (as well as of the entire flow) are artifact, considering the positive correlation between the LOD observation and the CAM variations estimated from large-scale magnetic field alone (Figure 9). If this is the case, it would support the significance of *Gillet et al.* [2010] coherency spectrum of their LOD prediction with respect to the observation. The spectrum shows a peak around the period of 6 years, at which the lag is nearly zero, even though their model is based on the strongly regularized magnetic field model gufm1 [*Jackson et al.*, 2000]. Presumably, flow perturbations due to randomly synthesized field are effectively eliminated by ensemble averaging process to obtain their model [see also *Gillet et al.*, 2009, Figure 13]. According to our analysis in section 4.2.1, the striking phase agreement for the 6 year oscillations in Figure 2 of *Gillet et al.* [2010] should arise from the large-scale ingredients of gufm1, but not to the prior assumptions they specifically impose, such as the quasi-geostrophy constraint.

Third, no full resolution of the flow variations is available, even if a perfect knowledge of SV up to degree 14 was given. In other words, the 6 year CAM variation is accompanied, to quite a good extent, by "invisible" flow variations or those involved in the null space of the practical flow inverse problem (Figure 11). In this regard the 6 year CAM variation contrasts with the decadal CAM variations, whose associated flow changes are actually due largely to "visible" flows [*Asari et al.*, 2009]. The decadal CAM fluctuations are more robustly recovered in our resolution tests as well. Also, according to our separate analysis of predicted LOD variations in frequency domain (Wardinski and Asari, submitted manuscript, 2015), no significant evidence of 6 year periodicity is found in the estimated CAMs, as opposed to those of around nine and longer years. The limited resolution for the 6 year CAM variation can even be more serious than the signal subtleness, as there is fundamentally no way to circumvent it.

As a final note, the amplitude of rapid CAM variation is subject to a substantial ambiguity. It can be underestimated due to the lack of resolution on one hand (Figure 11) or overestimated due to an imposition of tight constraints like TG on the other hand (the enhanced amplitude by the latter might yet be preferable for fitting the observed subdecadal LOD variation; see Figure 14 in *Pais and Jault* [2008], as well as Figure 8 in this paper, for quasi-geostrophy cases). While the inference of magnetic field intensity within the core [*Gillet et al.*, 2010] is not concerned with the amplitude of flow oscillation, its uncertainty matters when investigating the excitation sources of torsional oscillations or their coupling with the inner core and mantle [*Mound and Buffett*, 2005].

6. Concluding Remarks

We have assessed the variability of core angular momentum (CAM) variation computed according to the formulation by *Jackson et al.* [1993]. A number of core flow models are derived from the recent magnetic field model C^{3}FM2 by changing the inversion setting systematically. The estimated CAM variations are examined in the time domain for 1962.0 to 2008.0, with a particular focus on their relevance to the two specific features of the observed LOD variation: the trend over the half century and the 6 year oscillation.

With regard to the estimation of the CAM trend, we have revealed a general tendency for the core flow inversion setting. The estimated CAM trends become steeper as stronger constraints are used in the flow modeling. Most remarkably, a CAM trend consistent with the observed length of day (LOD) is still obtainable from a flow model strictly meeting the tight constraint of tangential geostrophy (TG). Such a flow model has to be built, so its predominant flows are not of planetary scale and that an interaction of unknown field and flow at small scales is allowed for in fitting the C^{3}FM2 secular variation. Under a more relaxed physical constraint of tangential magnetostrophy (TM), a CAM trend fitting the observed LOD trend emerges from a model dominated by planetary-scale flows. Separate interpretations can be made for these TG and TM flow models, each representing different states of the geodynamo that have been suggested by numerical dynamo simulations.

As for the estimation of the rapid CAM fluctuation, the phase is determined coherently from different flow models, no matter what constraints and regularizations are imposed on them. The estimated phase, which is also correlated with the subdecadal LOD observation, is inherent to the large-scale components of C^{3}FM2. However, we do not take this as sufficient evidence for robust detection of Earth's 6 year CAM oscillation. We rather have discussed multiple sources of the ambiguity. They are (a) variance of the modeled field,

(b) fluctuating magnetic field at smaller scales that are not modeled in C^{3}FM2, and (c) the theoretical lack of resolution in the core flow inversion. We have also discussed a chance of resolving the phase of 6 year CAM variation. Despite the unavoidable uncertainty (c), the estimated subdecadal CAM variations are roughly in phase with that of the observed 6 year LOD variation, even when they are derived from flow models built with a variety of inversion settings. A great advance in alleviating (a) is expected to be achieved by using a latest satellite field model. The irrelevance of (b) is suggested by the phase agreement discovered even for much cruder flow models that are estimated from C^{3}FM2 main field and secular variation truncated at as low spherical harmonic degree as 4. Also, the dispersion in the CAM variation estimation caused by synthetic field to account for (b) may be effectively canceled out by computing the ensemble average.

An additional finding would be the relative robustness of decadal CAM variation. The CAM fluctuations on these timescales are recognized commonly in almost every LOD prediction calculated from the numerous flow models estimated with a wide range of inversion setting. It is indicated that the decadal variation of zonal core flow is a better resolved feature than its trend, the amplitude of its subdecadal variations, or the flow itself.

Finally, we give a remark on the possibility of improving the current work. All our flow models adopted have been such as to fit the C^{3}FM2 secular variation on an equal level. We have measured this by a single quantity alone, i.e., the secular variation misfit root-mean-squared with respect to the Earth's surface and to the model period, in order to facilitate the computations of numerous inversions. A more detailed evaluation of the misfit could narrow the variability of flow models. For example, one would focus on explaining more precisely the westward drift at the core surface for discussing the CAM trend or on fitting directly the secular acceleration for discussing the rapid CAM variations. Such a treatment may give some hints at the issues still pending, e.g., specifying between TG and TM for the actual state of the Earth's core or revealing more firmly the presence of 6 year CAM variation and its contribution to the observed LOD fluctuation. The latter issue also concerns the generation mechanism of the observed 6 year periodicity of secular acceleration [*Silva et al.*, 2012]. Being a regional phenomenon at the core surface, this rapid periodicity may rather originate from a different mechanism than the torsional oscillations [*Chulliat and Maus*, 2014]. Considering the limit of numerical dynamos in resolving short timescale core dynamics [*Aubert*, 2014], observation-based studies should still play a primary role in the interesting task of finding out the physical connection or disconnection between the 6 year variations of Earth rotation and magnetic field.

Acknowledgments
R. Holme kindly provided his latest series of the excess LOD tuned for studying the core-mantle coupling. The authors would like to record their gratitude to M. Brown for improving the manuscript. This work is supported by German Research Foundation (DFG) within the frameworks of Research Grants and Priority Program1488 "Planetary Magnetism."

References

Amit, H., and M. A. Pais (2013), Differences between tangential geostrophy and columnar flow, *Geophys. J. Int.*, *194*, 145–157, doi:10.1093/gji/ggt077.

Asari, S., and V. Lesur (2011), Radial vorticity constraint in core flow modeling, *J. Geophys. Res.*, *116*, B11101, doi:10.1029/2011JB008267.

Asari, S., H. Shimizu, and H. Utada (2009), Robust and less robust features in the tangential geostrophy core flows, *Geophys. J. Int.*, *178*, 678–692.

Aubert, J. (2013), Flow throughout the Earth's core inverted from geomagnetic observations and numerical dynamo models, *Geophys. J. Int.*, *192*, 537–556, doi:10.1093/gji/ggs051.

Aubert, J. (2014), Earth's core internal dynamics 1840–2010 imaged by inverse geodynamo modelling, *Geophys. J. Int.*, *197*, 1321–1334, doi:10.1093/gji/ggu064.

Bloxham, J. (1988), The determination of fluid flow at the core surface from geomagnetic observation, in *Mathematical Geophysics: A Survey of Recent Developments in Seismology and Geodynamics*, edited by V. J. Vlaar et al., pp. 189–208, D. Reodel Publ. Comp., Hingham, Mass.

Brown, W. J., J. E. Mound, and P. W. Livermore (2013), Jerks abound: An analysis of geomagnetic observatory data from 1957 to 2008, *Phys. Earth Planet. Inter.*, *223*, 62–76.

Celaya, M., and J. Wahr (1996), Aliasing and noise in core-surface flow inversions, *Geophys. J. Int.*, *126*, 447–469.

Christensen, U. R., P. Olson, and G. A. Glatzmaier (1999), Numerical modelling of the geodynamo: A systematic parameter study, *Geophys. J. Int.*, *138*, 393–409.

Chulliat, A., and S. Maus (2014), Geomagnetic secular acceleration, jerks, and a localized standing wave at the core surface from 2000 to 2010, *J. Geophys. Res. Solid Earth*, *119*, 1531–1543, doi:10.1002/2013JB010604.

Eymin, C., and G. Hulot (2005), On core surface flows inferred from satellite magnetic data, *Phys. Earth Planet. Inter.*, *152*, 200–220.

Gillet, N., M. A. Pais, and D. Jault (2009), Ensemble inversion of time-dependent core flow models, *Geochem. Geophys. Geosyst.*, *10*, Q06004, doi:10.1029/2008GC002290.

Gillet, N., D. Jault, E. Canet, and A. Fournier (2010), Fast torsional waves and strong magnetic field within the Earth's core, *Nature*, *465*, 74–77.

Holme, R. (1998), Electromagnetic core-mantle coupling: II. Probing deep mantle conductance, in *The Core-Mantle Boundary Region, Geodynamics Ser.*, vol. 28, edited by M. Gurnis et al., pp. 139–151, AGU, Washington, D. C.

Holme, R. (2007), Large scale flow in the core, in *Treatise in Geophysics, Core Dynamics*, vol. 8, edited by R. Holme and G. Schubert, pp. 107–129, Elsevier, Amsterdam.

Holme, R., and O. de Viron (2005), Geomagnetic jerks and a high-resolution length-of-day profile for core studies, *Geophys. J. Int.*, *160*, 435–439.

Holme, R., and O. de Viron (2013), Characterization and implications of intradecadal variations in length of day, *Nature*, *499*, 202–204.

Holme, R., and N. Olsen (2006), Core surface flow modelling from high-resolution secular variaion, *Geophys. J. Int.*, *166*, 518–528.

Hongre, L., G. Hulot, and A. Khokhlov (1998), An analysis of the geomagnetic field over the past 2000 years, *Phys. Earth Planet. Inter.*, *106*, 311–335.
Hori, K., J. Wicht, and U. R. Christensen (2012), The influence of thermo-compositional boundary conditions on convection and dynamos in a rotating spherical shell, *Phys. Earth Planet. Inter.*, *196-197*, 32–48.
Hulot, G., J.-L. Le Mouël, and J. Wahr (1992), Taking into account truncation problems and geomagentic model accuracy in assessing computed flows at the core-mantle boundary, *Geophys. J. Int.*, *108*, 224–246.
Jackson, A. (1996), Kelvin's theorem applied to the Earth's core, *Philos. Trans. R. Soc.*, *A452*, 2195–2201.
Jackson, A. (1997), Time-dependency of tangentially geostrophic core surface motions, *Phys. Earth Planet. Inter.*, *103*, 293–311.
Jackson, A., J. Bloxham, and D. Gubbins (1993), Time-dependent flow at the core surface and conservation of angular momentum in the coupled core-mantle system, in *Dynamics of Earth's Deep Interior and Earth Rotation*, vol. 72, edited by J.-L. Le Mouël, D. E. Smylie, and T. Herring, pp. 97–107, AGU, Washington, D. C.
Jackson, A., A. R. T. Jonker, and M. R. Walker (2000), Four centuries of geomagnetic secular variation from historical records, *Philos. Trans. R. Soc.*, *A358*, 957–990.
Jault, D., C. Gire, and J.-L. Le Mouël (1988), Westward drift, core motion and exchanges of angular momentum between core and mantle, *Nature*, *333*, 353–356.
Le Mouël, J.-L. (1984), Outer-core geostrophic flow and secular variation of Earth's geomagnetic field, *Nature*, *311*, 734–735.
Lesur, V., I. Wardinski, M. Rother, and M. Mandea (2008), GRIMM: The GFZ Reference Internal Magnetic Model based on vector satellite and observatory data, *Geophys. J. Int.*, *173*, 382–394.
Lesur, V., I. Wardinski, S. Asari, B. Minchev, and M. Mandea (2010), Modelling the Earth's core magnetic field under flow constraint, *Earth Planets Space*, *62*, 503–516.
Mound, J. E., and B. A. Buffett (2005), Mechanisms of core-mantle angular momentum exchange and the observed spectral properties of torsional oscillations, *J. Geophys. Res.*, *110*, B08103, doi:10.1029/2004JB003555.
Mound, J. E., and B. A. Buffett (2006), Detection of a gravitational oscillation in length-of-day, *Earth Planet Sci. Lett.*, *243*, 383–389.
Olsen, N., and M. Mandea (2008), Rapidly changing flows in the Earth's core, *Nat. Geosci.*, *1*, 390–394.
Pais, A., and G. Hulot (2000), Length of day decade variations, torsional oscillations and inner core superrotation: Evidence from recovered core surface zonal flows, *Phys. Earth Planet. Inter.*, *118*, 291–316.
Pais, M. A., and D. Jault (2008), Quasi-geostrophic flows responsible for the secular variaion of the Earth's magnetic field, *Geophys. J. Int.*, *173*, 421–443.
Pais, M. A., O. Oliveira, and F. Nogueira (2004), Nonuniqueness of inverted core-mantle boundary flows and deviations from tangential geosgrophy, *J. Geophys. Res.*, *109*, B08105, doi:10.1029/2004JB003012.
Rau, S., U. Christensen, A. Jackson, and J. Wicht (2000), Core flow inversion tested with numerical dynamo models, *Geophys. J. Int.*, *141*, 485–497.
Sabaka, T., N. Olsen, and M. Purucker (2004), Extending comprehensive models of the Earth's magnetic field with Ørsted and CHAMP data, *Geophys. J. Int.*, *159*, 521–547.
Sakuraba, A., and P. H. Roberts (2009), Generation of a strong magnetic field using uniform heat flux at the surface of the core, *Nat. Geosci.*, *2*, 802–805.
Schaeffer, N., and M. A. Pais (2011), On symmetry and anisotropy of Earth-core flows, *Geophys. Res. Lett.*, *38*, L10309, doi:10.1029/2011GL046888.
Silva, L., L. Jackson, and J. Mound (2012), Assessing the importance and expression of the 6 year geomagnetic oscillation, *J. Geophys. Res.*, *117*, B10101, doi:10.1029/2012JB009405.
Sreenivasan, B., and C. A. Jones (2006), The role of inertia in the evolution of spherical dynamos, *Geophys. J. Int.*, *164*, 467–476.
Wardinski, I. (2005), Core surface flow models from decadal and subdecadal secular variation of the main geomagnetic field, PhD thesis, Freie Univ., Berlin.
Wardinski, I., and V. Lesur (2012), An extended version of the C^3FM geomagnetic field model: Application of a continuous frozen-flux constraint, *Geophys. J. Int.*, *189*, 1409–1429.
Wardinski, I., R. Holme, S. Asari, and M. Mandea (2008), The 2003 geomagnetic jerk and its relation to the core surface flows, *Earth Planet Sci. Lett.*, *267*, 468–481.